Asian Journal of Science, Engineering and Technology (AJSET)
eISSN: 3006-6980 (online)
https://ideapublishers.org/index.php/ajset
Vol. 4, No. 1 (January-June), 2025, pp. 69-86
https://doi.org/10.47264/idea.ajset/4.1.5
Original Research Article

Evaluating the engineering design and computational analysis: a case study of Machai micro-hydropower plant, Mardan, Pakistan

Uzair Ali[1] | Adnan Nawaz[1] | Abdul B Mansoor[2] | Arif Usman[3] | M Junaid Iqbal[4] | Fahad Ali[5]

1. Local Government and Rural Development Department, Khyber Pakhtunkhwa, Pakistan.
2. Pakistan Public Works Department, Ministry of Housing and Works, Punjab, Pakistan.
3. CECOS University of Information Technology and Emerging Sciences, Peshawar, Pakistan.
4. University of Engineering and Technology, Bannu, Khyber Pakhtunkhwa, Pakistan.
5. Quaid-e-Awam University of Engineering, Science and Technology, Nawabshah, Pakistan

*Corresponding Author Email: engruzair91@gmail.com

Article History

Received:
10-Apr-2025

Revised:
05-May-2025

Re-revised:
13-Jun-2025

Accepted:
13-Jun-2025

Published:
21-Jun-2025

Abstract: Hydroelectric power generation is one of the most significant and dependable renewable energy sources for Pakistan. With a few minor adjustments and a range of design options, micro hydropower plants may be built on an existing canal to restore or boost irrigation water delivery and generate electricity by choosing the appropriate turbine. The design of the Machai hydropower plant was examined in this study using the Manning equation to establish the power canal's design specifications. The Manning roughness coefficient is calculated to find the section factor. Hydraulic mean depth, top width, height, area, and channel width may all be determined using the section factor. Based on the outcomes of the TURBNPRO program, the Kaplan turbine installed in the powerhouse was selected. To evaluate the stability of embankments, SLIDE software was employed. The study concludes that micro-hydropower is a technically viable and environmentally friendly method of producing electricity in remote areas. Particularly for isolated off-grid locations, Machai and other micro-hydropower devices provide a cost-effective and ecologically friendly energy alternative. Compared to diesel generators or coal-fired power plants, micro-hydropower is a more environmentally beneficial choice since it emits no greenhouse gases when in operation.

Keywords: Hydropower plant, Kaplan turbine, Power canal, Manning coefficient, Remote areas, Hydraulic parameters, Hydroelectric power, Power generation, Renewable energy.

How to Cite: Ali, U., Nawaz, A., Mansoor, A. B., Usman, A., Iqbal, M. J., & Ali, F. (2025). Evaluating the engineering design and computational analysis: a case study of Machai micro-hydropower plant, Mardan, Pakistan. *Asian Journal of Science, Engineering and Technology (AJSET), 4*(1), 69-86. https://doi.org/10.47264/idea.ajset/4.1.5

1. Introduction

The hydropower system transforms the potential energy of a volume of water flowing in a stream with a certain degree of fall to the turbine, known as the head, into electric energy at the bottom of the system, where the powerhouse is located. A hydroelectric plant's output power is proportional to its head and flow (Karre *et al.*, 2022; Anaza *et al.*, 2017; Yah *et al.*, 2017; Loots *et al.*, 2015).

Depending on their location, the sort of grid that distributes energy, their load capacity, and the type of storage they utilise, hydropower systems are categorised in many ways. The most often recognised classification, however, is based on the capacity to produce power (Dametew, 2016). The term "micro HPP" describes hydropower facilities that produce less than 100 kW of electricity. By contrast, "mini HPP" means those that produce 100–1000 kW, "small HPP" means those that produce 1–10 MW, “medium HPP” means those that produce 10–300 MW and "large HPP" means those that produce more beyond 300 MW (Mukwindi, 2019). Using computational analytical techniques, the engineering design of the Machai Micro-Hydropower Plant exhibits a great degree of efficacy and efficiency, as the article title emphasises. It has been possible to precisely describe and optimise the hydraulic and structural components of the plant via the use of sophisticated computational techniques, including Finite Element Analysis (FEA) and Computational Fluid Dynamics (CFD) simulations. Engineers were able to analyse flow behaviour, detect energy losses in the system, and mimic real-world operating situations thanks to these technologies. Changes to the design might thus be made early on to improve performance and cut down on inefficiencies. Optimising the turbine shape and penstock dimensions, increasing energy conversion efficiency, and lowering construction and maintenance costs were all made possible by the computer study. Its contextual significance and sustainability are further highlighted by the design's flexibility in responding to the terrain and hydrological features of the Machai region. A paradigm for future micro-hydropower developments in comparable terrains, the Machai micro-hydropower plant's performance, dependability, and cost-effectiveness were all greatly enhanced by the use of computer analysis in the engineering design process.

A stream or canal directs water into a pipeline, which the turbine uses to move the water downhill or down the slope. This is the basic principle that underlies the functioning of a hydroelectric system. The pressure at the pipeline's bottom is generated by the vertical drop (HEAD). The turbine is propelled by the force produced by the pressure of water exiting the pipe's end, which converts the water power into rotational power through the shaft. The waterpower is subsequently transformed into electrical power by the powerhouse's generator, which is either fed into the grid or, in the case of a micro-hydro plant, provided to the neighbourhood. Friction causes some of the energy generated to be lost at each step of the conversion process. The quantity of energy converted after considering the frictional losses is the system's total efficiency. Every component of the hydro system affects the plant's performance, from water input to turbine-generator alignment (Committee of Hydropower Intakes, 2014).

The maximum discharge that the power canal can carry is determined by the design flow of the hydro system. The Manning Equation, Chezy Equation, Lacey regime theory, and Khosla's theory are some of the design decisions made for an existing canal to build a power canal. The Manning equation is the most reliable and often used formula for power canal development. The Manning equation uses the cross-sectional area of flow, the wetted perimeter of flow, the

slope of the channel bed, and the surface roughness of the channel to determine the flow velocity (Yah *et al.*, 2017). Researchers used HOMER-Pro and genetic algorithms to analyse a hybrid system that combines solar energy, grid power, and micro-hydro. The Net Present Cost (NPC) of a hydro-to-grid system was 23% less than that of hybrid alternatives. Moreover, opt-sized trigeneration (hydro-solar-grid) decreased solar-grid expenses by 50% and NPC by 36%. Undershot waterwheel turbines were designed and optimised using SolidWorks CAD and ANSYS CFD. Prototype testing confirmed the accuracy of CFD-based blade profiling. In the field, crossflow turbines were assessed at head sites of around 10 meters. With an average efficiency of around 67.6%, the power outputs varied from roughly 8.5 to 48.6 kW. The efficiency of well-built sites was much higher than that of poorly matched ones.

To prevent scouring and silting, irrigation canals are constructed with a specific permissible bed slope. However, because of the uneven terrain slope, it is not always possible to achieve the desired canal bed slope along the entire alignment. To avoid unnecessary large-scale earth-filling activities, a vertical drop or canal fall is provided to step down the canal bed. This step-down is then continued with an acceptable slope until another step-down is needed. Installing turbines for power generation is made possible by these drops and falls, which provide the head required for maximum efficiency (Loots *et al.*, 2015). The canal is lengthened to accommodate the intake and overflow to construct a hydropower plant. Usually, an extended spillway is built to reduce the width of the intake. A penstock that travels down the canal brings the water from the intake under pressure to the turbine. After passing through the turbine, the water returns to the river through a brief tailrace (Dametew, 2016).

Figure 1: illustration of hydropower system installed on an existing canal

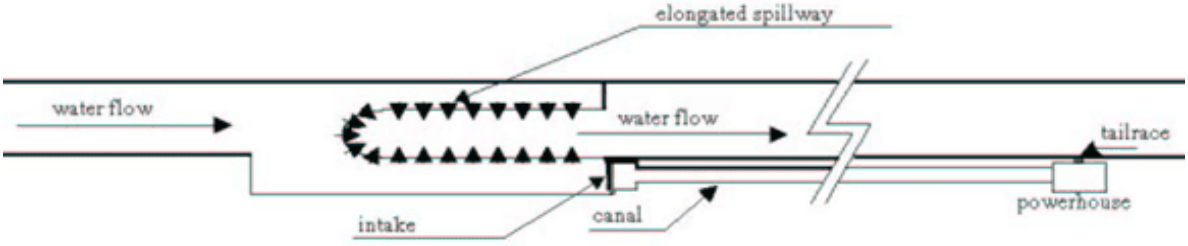

The essential part of the hydropower system is the turbine. Converting fluid energy (water) into mechanical energy is the turbine's main job. This mechanical energy is then used to run a generator in a power plant. Combining a hydro turbine and a hydro generator creates the hydraulic power unit, which determines how much electricity is generated overall. Achieving maximum efficiency requires choosing the right turbine (Mukwindi, 2019). The hydraulic head, flow rate, and site-specific requirements—such as the quantity and kind of units, capacity, speed, turbine efficiency, and cost—all influence the turbine choice. The two main types of turbines used in hydropower plants are impulse and reaction turbines. Many authors investigated numerous RS techniques for monitoring and assessing groundwater supplies. LANDSAT VIII satellite imagery is used in this research to extract LULC data. This imagery is useful for studying the spatial distribution of various land cover types, which influences GWR (Zaheer *et al.*, 2025; Mahmood *et al.*, 2024; Tufail *et al.*, 2024; Pasha *et al.*, 2025; Anjum *et al.*, 2025).

The Pelton wheel illustrates the Impulse Turbine, which is suitable for situations with high head and low flow. Converting the kinetic energy of a high-velocity water jet into mechanical energy is the basic purpose of an impulse turbine (Židonis *et al.*, 2015). While reaction turbines,

like the Francis and Kaplan types, are best suited for sites with medium to low heads and high flow conditions, impulse turbines perform exceptionally well in areas with high hydraulic heads and relatively low flow rates. The conversion of water's kinetic and potential energy into mechanical energy is one of the basic ideas behind how these turbines work. Kaplan turbines work best in low-head, high-flow situations, while Francis turbines can handle a range of heads and flow rates (Elbatran *et al.*, 2015; Kaunda *et al.*, 2014).

Table-1: Type of turbine based on net head

Range of heads Turbine type	Head range in meters
Kaplan and Propeller	$2 < H_n < 40$
Francis	$25 < H_n < 350$
Pelton	$50 < H_n < 1'300$
Crossflow	$5 < H_n < 200$
Turgo	$50 < H_n < 250$

Figure 2: Type of turbine based on discharge

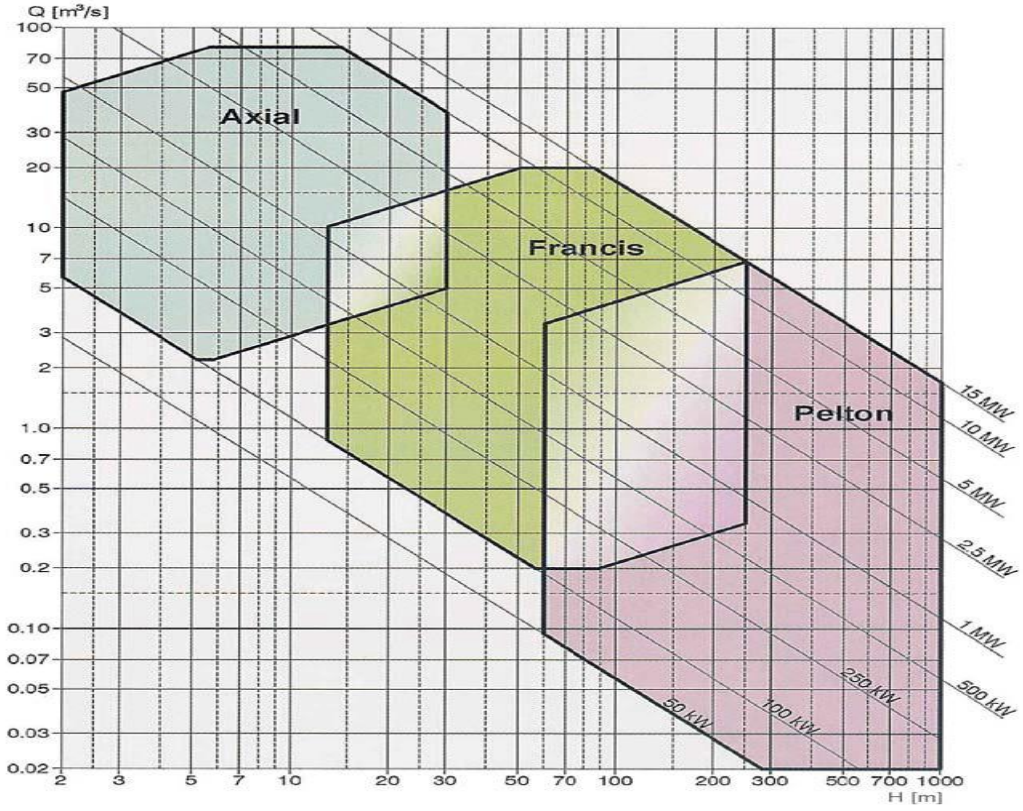

A key component of a hydropower system's overall performance is the turbine's efficiency. The runner's design, material quality, and operating conditions all have an impact on a turbine's efficiency. Modern turbines are designed to achieve efficiencies of above 90%, but the true efficiency depends on the specific site conditions and installation quality (Thapa *et al.*, 2015; Jain *et al.*, 2015). According to the literature assessment, the best selection criterion for the turbine is the power canal's design, which is determined by the Manning equation and the available nett water head. This criterion was also used in the Machai hydropower plant's design assessment, and TURBNPRO 3 software—a programme for hydraulic turbine sizing and

technical data development—was used to further validate the turbine selection that was installed on-site. Preferred operating settings, anticipated equipment configuration, and hydroelectric site characteristics are the input data that this software uses to function. Based on their typical characteristics, hydraulic turbine systems' sizes, speeds, operational limitations, dimensions, and performance characteristics are presented in this text.

Examining the Machai Micro-Hydropower Plant's engineering design and computational analysis critically is the study's goal. This study's focus is on a particular micro-hydropower facility in Machai, Pakistan. The study is limited by the data and tools available to design parameters, simulation models, and operational efficiency.

2. Research methodology and calculations

The design evaluation of small hydropower plants and their associated factors, including power canal design, turbine selection for power generation, and canal embankment stability analysis, is the main focus of this study. With the head race at RD 50+537 (with falls at RD 51+100, RD 51+272, and RD 51+786) and the tail race at RD 52+100, the project is located along the Machai Canal in the Mardan district of Khyber Pakhtunkhwa, Pakistan. Starting at the Amandara Headworks on the Swot River, the Machai Canal is a part of the Upper Swot Canal System. Figure 3 shows the powerhouse located at 34°25'12 "N 72°02'43 “E.”

Figure 3: Location map of the study area

2.1. Project overview

The hydroelectric plant, which provides energy to a private steel industry, was created through a public-private partnership based on nett metering. There are no obstructions in the main Machai canal. The powerhouse is located at RD 51+450 on the central canal's right bank. On the right side of the central canal is a connected power canal that runs from RD 50+537 to RD 52+000.

Table-2: Salient features of Machai Hydropower Plant

Properties	**Values**
Location	Machai Canal Mardan
Discharge	40 m^3/s
Capacity	2.2 MW
Length	200 m
Lining	Concrete Lining over Grouted Rip Rap
No. of Units	2
Unit Capacity	1.1 MW each
Turbines Type	Vertical axes Kaplan
Available Net Head	6 m
Annual Energy Output	8 GWh

The powerhouse is located close to the middle of the connecting channel, and cross regulators are used to send the discharge from the central canal to the powerhouse via the connecting power canal. Before a controlled structure that serves as a diversion wall at RD 50+537, the project features a headrace channel that emerges from the Machai Canal. This headrace canal's design discharge of 40 m^3/s is redirected to the powerhouse on the Machai Canal's right side. The project's key features and layout are presented in Table-2 and Figure 4 below.

Figure 4: Layout of Machai Hydropower Plant

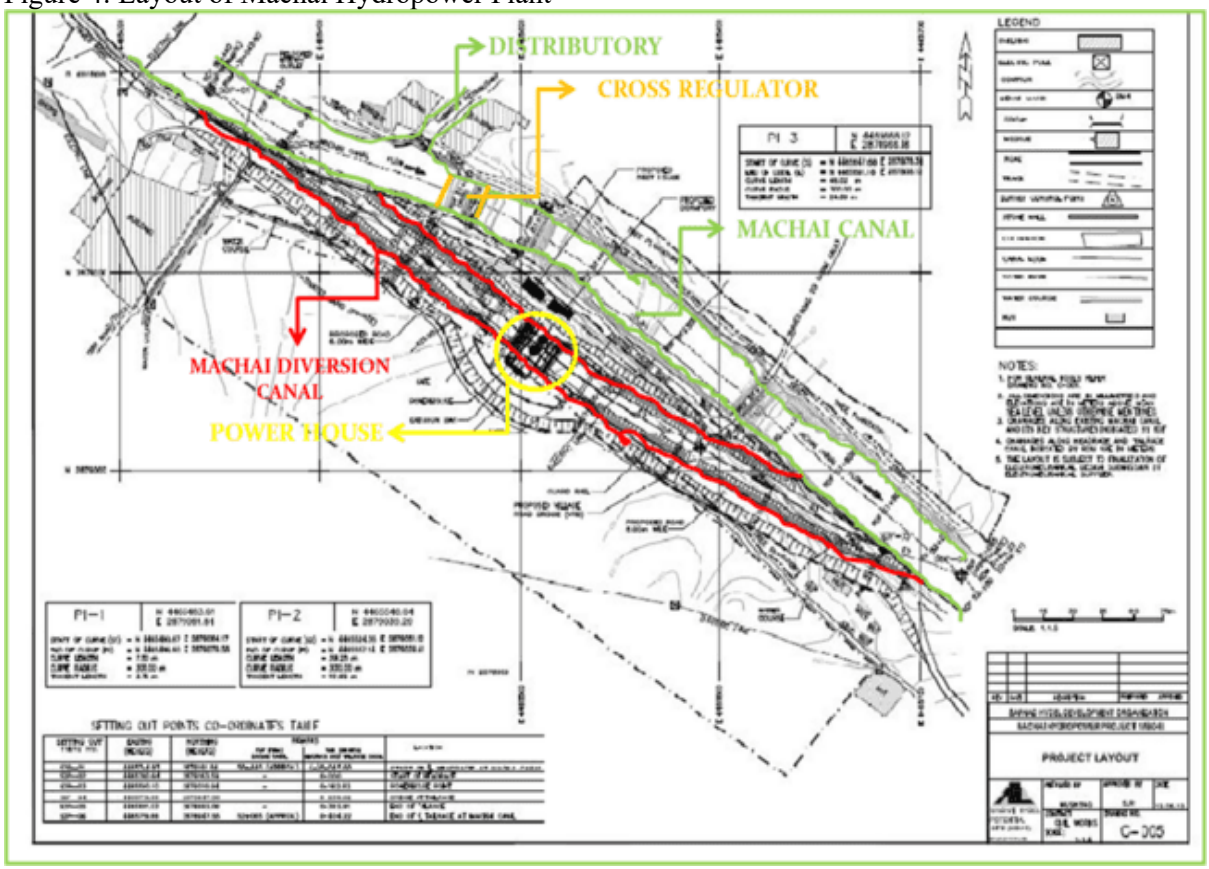

2.2. Calculation of hydraulic parameter

The calculation of various hydraulic parameters was conducted utilising the Manning Equation. The Machai hydropower plant is designed for a discharge of 40m³/s with a longitudinal slope of the Machai Canal measuring 0.0002. Based on the provided table, the estimate of Manning's roughness coefficient is 'n'.

Table-3: Manning roughness coefficient 'n'

Lining	Lining Type	n-value	Different depth	Ranges
Category			Depth ranges	
		0 15 cm	15 - 60 cm	> 60 cm
	Concrete	0.015	0.013	0.013
	Grouted Riprap	0.040	0.030	0.028
	Stone Masonry	0.042	0.032	0.030
Rigid	Soil Cement	0.025	0.022	0.020
	Asphalt	0.018	0.016	0.016
	Bare Soil	0.023	0.020	0.020
Unlined	Rock Cut	0.045	0.035	0.025
	Woven Paper Net	0.016	0.015	0.015
	Jute Net	0.028	0.022	0.019
	Fiberglass Roving	0.028	0.021	0.019
	Straw with Net	0.065	0.033	0.025
Temporary	Cured Wood Mat	0.066	0.035	0.028
	Synthetic Mat	0.036	0.025	0.021
Gravel	2.5-cm (d50)	0.044	0.033	0.030
Riprap	5 -cm (d50)	0.066	0.041	0.034
Rock	15-cm (d50)	0.104	0.069	0.035
Riprap	30-cm (d50)	-	0.078	0.04C

The roughness coefficient for the Machai Hydropower site II concrete lining is 0.015. Computation of value of section factor using Manning equation (For the calculation of the various design parameters for both head and tail race, we will be considering half of the width of the channel)

$$A = 1.73y^2 \quad P = 3.46\text{y} \quad R = \frac{y}{2}$$

$$Q = \frac{1}{n}\left(A(R)^{2/3}(S_o)^{1/2}\right)$$

$$40 = \frac{1}{0.015}\left(1.73y^2\left(\frac{y}{2}\right)^{2/3}(0.0002)^{1/2}\right)$$

$$y^{8/3} = 38.92$$

$y = 3.94$

Width of Trapezoidal channel,

$b = 1.15\ y$

$b = 4.5\ m$ The total width of the channel $B = 2 \times b = 9\ m$

Area,

$A = 1.73(3.94)^2$

$A = 26.85\ m^2$

Parameter,

$P = 3.46(3.94)$

$P = 13.63\ m$

Hydraulic Radius,

$R = \frac{3.94}{2}$

$R = 1.97\ m$

Velocity

$V = \frac{Q}{A}$

$V = 1.5\ m/s^2$

Top Width

$t = 4/\sqrt{3}(3.94)$

$t = 9.09\ m$

Total Top Width $T = 2 \times t = 18.2\ m$

Hydraulic Mean Depth

$D = \frac{26.85}{9.09} = 2.95\ m$

For Q = 40m^3/s, we assume a freeboard of 0.9 m

Total Depth = y + freeboard

Total Depth = 4.85 m

2.3. Design of spillway

The dimension of the spillway is given by,

$L_{spillway} = (Q_{flood} - Q_{design})/C_w(h_{flood} - h_{sp})^{1.5}$ (Pandey, 2011)

Where,

$L_{spillway}$ = Length of the spillway (m)
Q_{flood} = Flood flow via intake (m^3/s)
Q_{design} = Design flow in headrace canal (m^3/s)
h_{flood} = Height of the flood level in the canal (m)
h_{sp} = Height of the spillway crest from the canal bed (m)
$h_{overtop}$= h_{flood}-h_{sp}

Based on the field data of the Machai Canal, the design flow (Q_{design}) is 40 m^3/s during the regular season. Similarly, the flow (Q_{flood}) reaches 63 m^3/s during the flood season. By conventional design, $h_{overtop}$ is taken as 1.17 m.

According to the survey, the height of the flood level in the canal is 2.7 meters. The only other value in the equation that needed to be determined is the length of the spillway Cw or the coefficient for a road-crested weir with round edges. This is generally used for constructing Micro Hydro Projects, and its value is considered to be 1.6.

For the design of the spillway, an assumption is to be considered what would be the Length required if the design flow was 0 m^3/s.

Cw = 1.6
Q_{flood} = 63 m^3/s
Q_{design} = 0 m^3/s
$h_{overtop}$= h_{flood}-h_{sp} = 1.17 m by convention.

In this case, the length of the spillway would be,

$L_{spillway} = (Q_{flood} - Q_{design})/C_w(h_{flood} - h_{sp})^{1.5}$ = (63-0) / 1.6 $(1.17)^{1.5}$ = 31.5 m

However, it is also necessary to calculate the length of the spillway by considering the actual flow of water that enters through the orifice and the head race canal. In that case,

Cw = 1.6
Q_{flood} = 63 m^3/s
Q_{design} = 40 m^3/s
$h_{overtop}$= h_{flood}-h_{sp} = 100 mm by convention.

In this case, the length of the spillway would be,

$$L_{spillway} = (Q_{flood} - Q_{design})/C_w\left(h_{flood} - h_{sp}\right)^{1.5} = (63\text{-}40) / 1.6\ (1.17)^{1.5} = 11.4\ \text{m}$$

Figure 5: Layout of Machai power canal

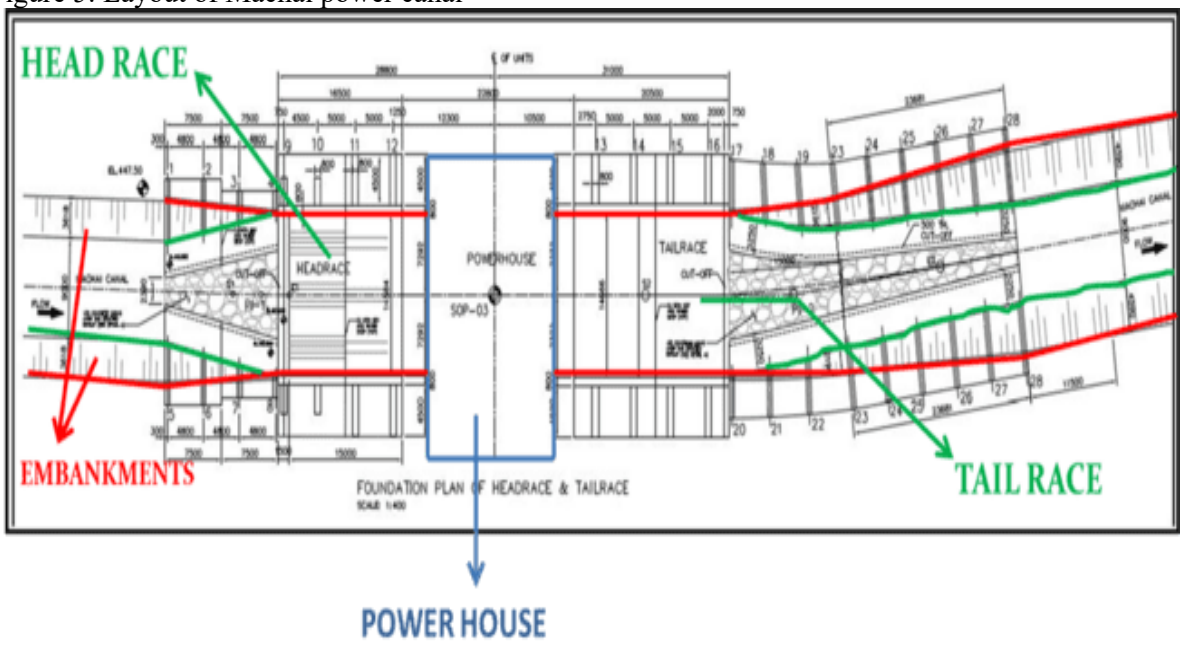

3. Stability analysis of spillway

Evaluating the stability of the slopes on either side of the power canal embankment is necessary for the stability analysis of the embankments (Karmakar *et al.*, 2021; Kovrov & Prychyna, 2017). Slide software, version 6, is used to perform the slopes' stability study. The material qualities used in the embankment's construction, the angle of internal friction, cohesion, the type of lining laid over the slope, and the amount of water within the embankment are all crucial parameters for performing stability analysis in the software (Ghumman *et al.*, 2020; Sasthav & Oladosu, 20222, Mayeda & Boyd, 2020).

Figure 6: Embankments of power canal

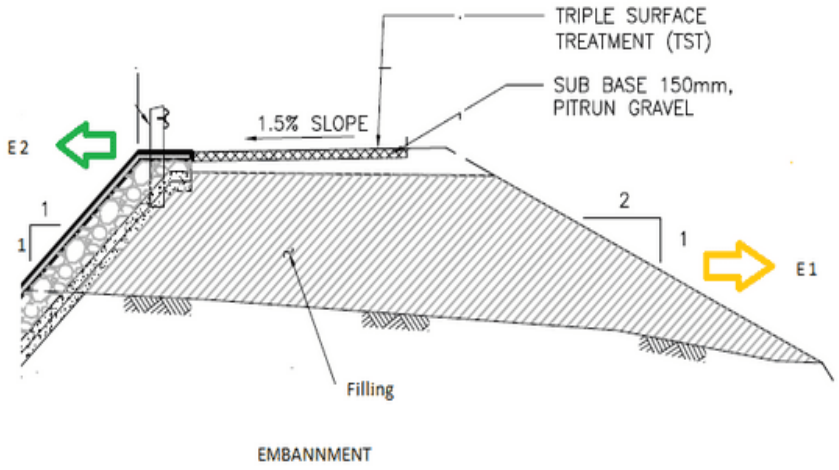

The analysis indicates that the lowest safety factor for the critical slip surface exceeds 2.5. Therefore, the Machai hydropower embankments are deemed stable and are not expected to fail under water pressure or traffic loading.

Figure 7: Stability analysis of slope E1 (without lining) on the outer side

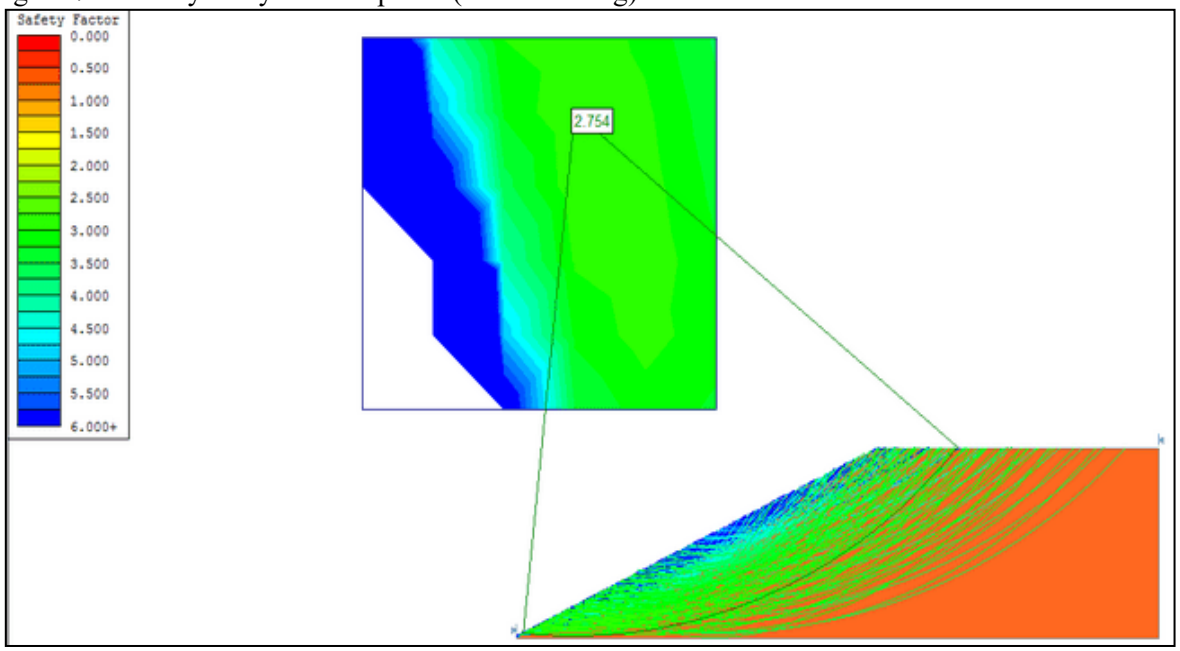

Figure 8: Stability analysis of slope E2 (with lining) on the inner side

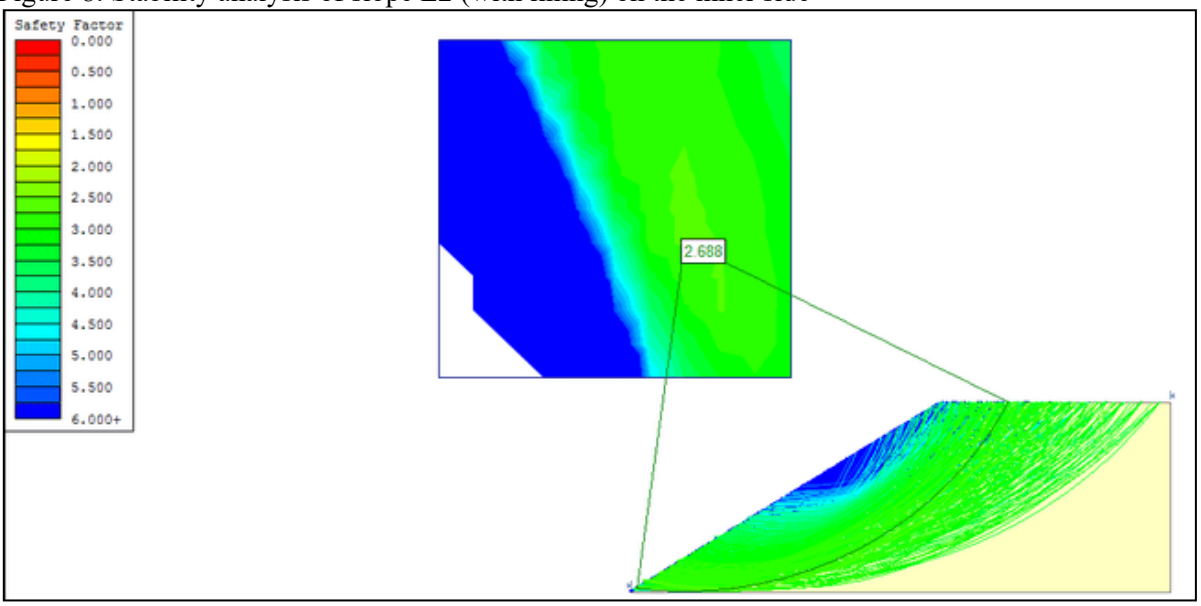

4. Selection of a turbine for power generation

Based on the site conditions and the available nett head of 6 metres, the Kaplan (axial/propeller) turbine is identified as the most suitable option for installation in the powerhouse to achieve efficient energy generation. The selection undergoes additional verification through the Turbn Pro 3 software (Sattar *et al.*, 2022; Asim *et al.*, 2022; Jamal & Khattak, 2021).

The turbine's power output at various available discharges has been assessed, yielding results that closely align with the values calculated during the feasibility study of the Machai Hydropower Plant. This confirms that the Kaplan turbine exhibits the highest energy efficiency in this scenario.

Figure 9: Turbine selection based on net available head

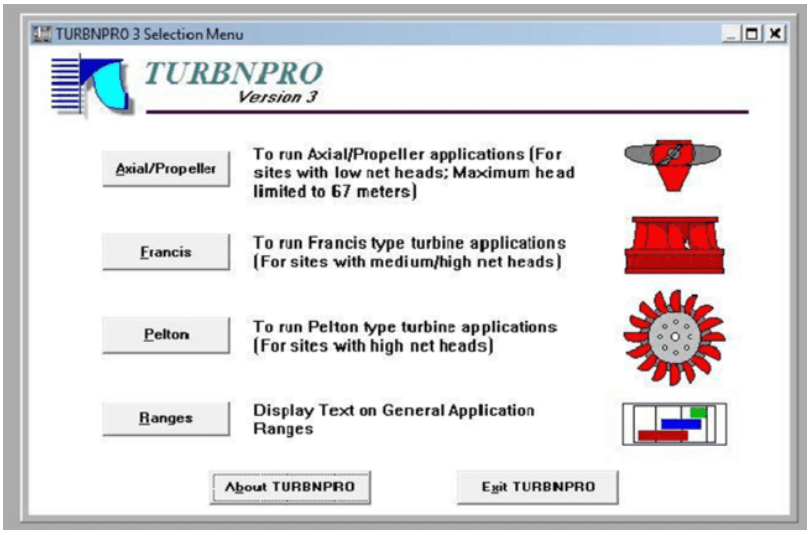

Figure 10: Site data for Machai Hydropower plant

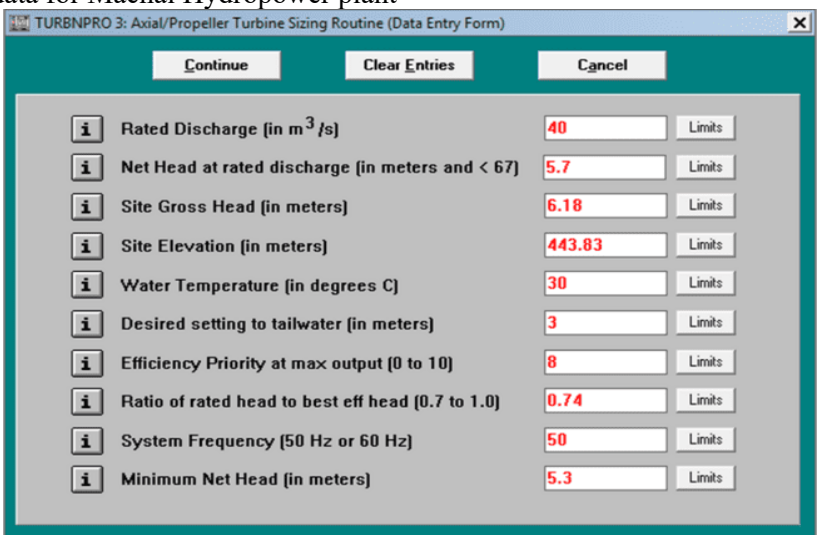

Figure 11: Turbine configuration

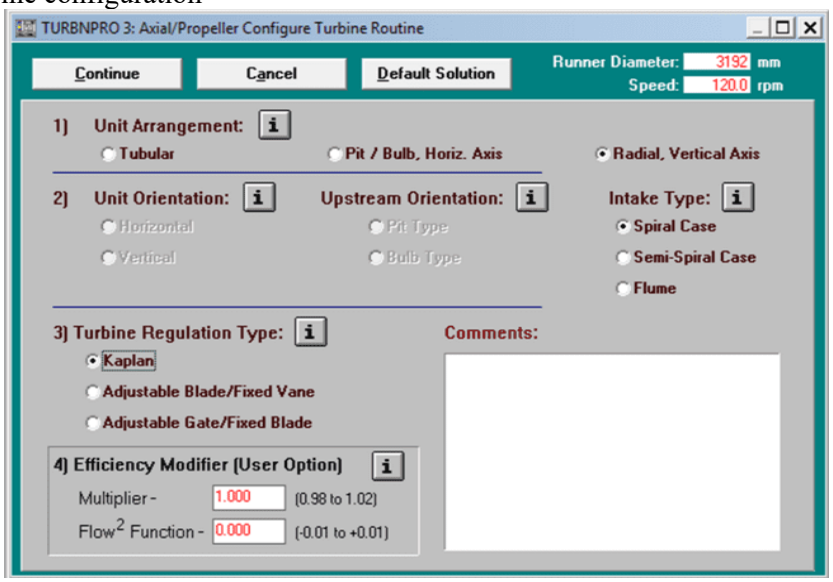

Figure 12: Summary of turbine power output at different discharges

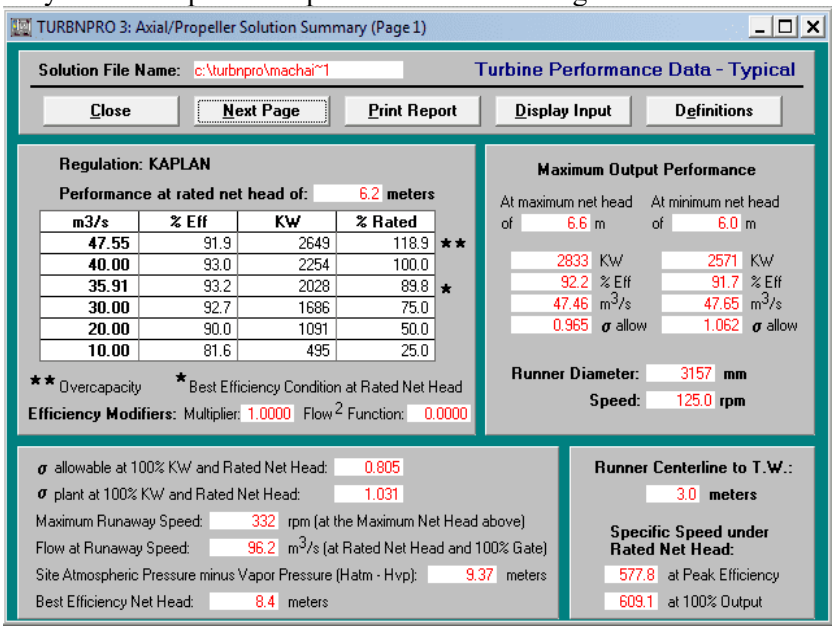

Figure 13: Turbine dimensions

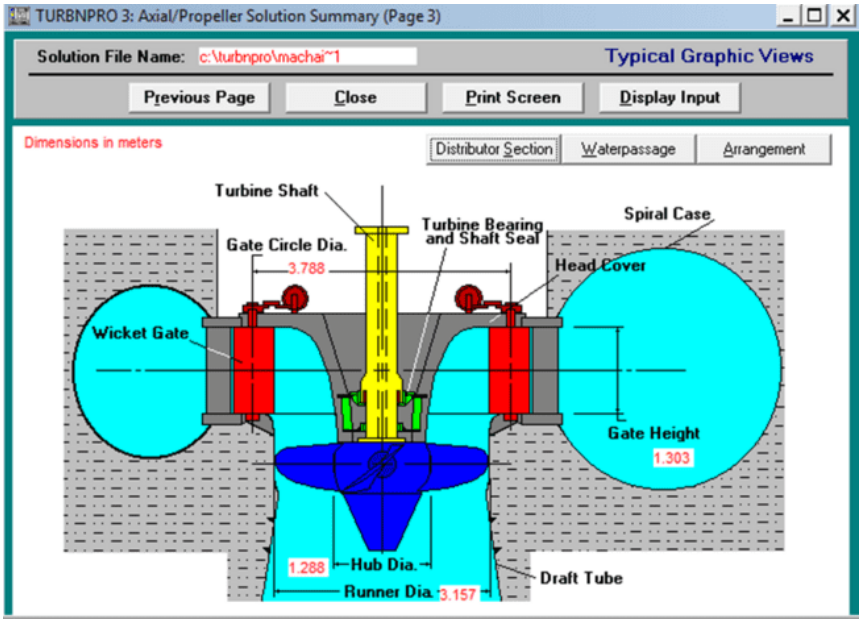

5. Conclusion

The study concludes that hydropower systems are significantly influenced by location-specific characteristics, which are evident from the practical design choices made for various components. The Machai hydropower plant was designed as a run-of-the-river type because it relies entirely on the Swat River, which flows through mountainous terrain, to supply water to the Machai canal. Run-of-the-river plants utilise the river's natural flow to generate energy and cease operation when water flow drops below the turbine's minimum operational requirement. The selection of materials for components such as the headrace canal, tailrace, and spillway was guided by the topographic conditions and the local availability of resources. Grouted riprap masonry with concrete lining was used at the headrace and tailrace as a dual filter layer to retain liner materials, prevent leakage from the canal linings, enhance embankment stability, and

ensure efficient water discharge. Simulations conducted using Turbnpro software validated that the two Kaplan turbines installed in the powerhouse enable the plant to operate effectively even during low winter discharge periods. The research also affirms that small hydropower projects provide a cost-effective, clean, and greenhouse gas-free energy solution for local communities. Furthermore, by leveraging the energy potential within Pakistan's extensive irrigation canal network, such micro and small-scale hydropower systems can be replicated across the country to help mitigate the national electricity shortfall.

Declaration of conflict of interest

The author(s) declared no potential conflicts of interest(s) with respect to the research, authorship, and/or publication of this article.

Funding

The author(s) received no financial support for the research, authorship and/or publication of this article.

ORCID iD:

Uzair Ali https://orcid.org/0009-0007-7341-8589

Adnan Nawaz https://orcid.org/0009-0005-9281-1023

Abdul Basit Mansoor https://orcid.org/0009-0007-4907-2987

Arif Usman https://orcid.org/0009-0002-5555-7773

Muhammad Junaid Iqbal https://orcid.org/0000-0001-6939-0180

Fahad Ali https://orcid.org/0009-0006-8578-4001

Publisher's Note

IDEA Publishers Group (AJSET IDEA-PG) stands neutral with regard to the jurisdictional claims in the published maps and the institutional affiliations.

References

Bandyopadhyay, O., Biswas, A., & Bhattacharya, B. B. (2016a). Classification of long-bone fractures based on digital-geometric analysis of X-ray images. *Pattern Recognition and Image Analysis, 26*, 742–757. https://doi.org/10.1134/S1054661816040027

Bandyopadhyay, O., Biswas, A., & Bhattacharya, B. B. (2016b). Long-bone fracture detection in digital X-ray images based on digital-geometric techniques. *Computer Methods and Programs in Biomedicine*, *123*, 2–14. https://doi.org/10.1016/j.cmpb.2015.09.013

Bhangare, Y., Rajeswari, K., & Game, P. S. (2024). Wrist bone fracture classification using least entropy combiner for ensemble learning. *Journal of Engineering Science & Technology Review, 17*(3), 45–51. https://doi.org/10.25103/jestr.173.06

Brown, J. P., Engelke, K., Keaveny, T. M., Chines, A., Chapurlat, R., Foldes, A. J., ... & Libanati, C. (2021). Romosozumab improves lumbar spine bone mass and bone strength parameters relative to alendronate in postmenopausal women: results from the Active-Controlled Fracture Study in Postmenopausal Women with Osteoporosis at High Risk (ARCH) trial. *Journal of Bone and Mineral Research*, *36*(11), 2139-2152.

Dell'Osa, A. H., Felice, C. J., & Simini, F. (2019). Bioimpedance and bone fracture detection. *Journal of Physics: Conference Series,* 1272. https://doi.org/10.1088/1742-6596/1272/1/012010

Deokar, N. D., & Thakur, A. G. (2016). Design, development and analysis of femur bone by using rapid prototyping. *International Journal of Engineering Development and Research, 4*(3), 881–886. https://rjwave.org/IJEDR/papers/IJEDR1603142

Deshmukh, S., Zalte, S., Vaidya, S., & Tangade, P. (2015). Bone fracture detection using image processing in Matlab. *International Journal of Advent Research in Computer and Electronics (IJARCE)*, 15–19.

Devi, M. S., Aruna, R., Almufti, S., Punitha, P., & Kumar, R. L. (2024). Bone feature quantisation and systematised attention gate UNet-based deep learning framework for bone fracture classification. *Intelligent Data Analysis,* (Preprint), 1–29. https://content.iospress.com/articles/intelligent-data-analysis/ida240431

Edward, C. P., & Hepzibah, H. (2015). A robust approach for detection of the type of fracture from x-ray images. *International Journal of Advanced Research in Computer and Communication Engineering, 4*(3), 479–482.

Ganesan, P., Sivakumar, S., & Sundar, S. (2015). A Comparative study on MMDBM classifier incorporating various sorting procedure. *Indian Journal of Science and Technology, 8*(9), 868. https://doi.org/10.17485/ijst/2015/v8i9/53064

Gonzalez, C. I., Melin, P., Castro, J. R., Mendoza, O., & Castillo, O. (2016). An improved sobel edge detection method based on generalised type-2 fuzzy logic. *Soft Computing, 20*, 773–784. https://doi.org/10.1007/s00500-014-1541-0

Hareendranathan, A. R., Tripathi, A., Panicker, M. R., Zhang, J., Boora, N., & Jaremko, J. (2023). Deep learning approach for automatic wrist fracture detection using ultrasound bone probability maps. *SN Comprehensive Clinical Medicine, 5*(1), 276.

Hasnain, M. A. (2023). Deep learning-based classification of dental disease using X-rays. *Journal of Computing & Biomedical Informatics, 5*(01), 82–95. https://www.jcbi.org/index.php/Main/article/view/141

Jabbar, J., Hussain, M., Malik, H., Gani, A., Khan, A. H., & Shiraz, M. (2022). Deep learning based classification of wrist cracks from X-ray imaging. *CMC-Computers Materials & Continua, 73*(1), 1827–1844.

Johnson, B., Alizai, H., & Dempsey, M. (2021). Fast field echo resembling a CT using restricted echo-spacing (FRACTURE): a novel MRI technique with superior bone contrast. *Skeletal Radiology*, *50*, 1705-1713.

Kaur, H. & Jain, A. (2017). Detection of Fractures in Orthopedic X-Ray Images. *International Journal of Advanced Research in Computer Science, 8*(3), 545–551. https://www.researchgate.net/publication/352438797

Khan, M., Sirdeshmukh, S. P. S. M. A., & Javed, K. (2016). Evaluation of bone fracture in animal model using bio-electrical impedance analysis. *Perspectives in Science, 8*, 567–569. https://doi.org/10.1016/j.pisc.2016.06.022

Khatik, I. (2017). A study of various bone fracture detection techniques. *Int J Eng Comput Sci, 6*(5), 21418–21423.

Kishor, K., Sengar, A., Sharma, A., & Gautam, D. (2025). Osteo fracture identification using deep learning techniques. *Health Services and Outcomes Research Methodology,* 1–40. https://doi.org/10.1007/s10742-025-00340-1

Lanka, S. R., & Yarramalle, S. (2018). Bone fracture identification-a case study based on statistical modelling. *International Journal of Advanced Research in Computer Science, 9*(1). https://doi.org/1010.26483/ijarcs.v9i1.5326

Muchtar, M. A., Simanjuntak, S. E., Rahmat, R. F., Mawengkang, H., Zarlis, M., Sitompul, O. S., ... & Nasution, T. H. (2018, March). Identification tibia and fibula bone fracture location using scanline algorithm. *Journal of Physics: Conference Series, 978*, 012043. https://doi.org/10.1088/1742-6596/978/1/012043

Naeem, A., Khan, A. Haider., Ayubi, S., & Malik, H. (2023). Predicting the metastasis ability of prostate cancer using machine learning classifiers. *Journal of Computing & Biomedical Informatics, 4*(02), 1–7. https://www.jcbi.org/index.php/Main/article/view/139

Nowroozi, A., Salehi, M. A., Shobeiri, P., Agahi, S., Momtazmanesh, S., Kaviani, P., & Kalra, M. K. (2024). Artificial intelligence diagnostic accuracy in fracture detection from plain radiographs and comparing it with clinicians: a systematic review and meta-analysis. *Clinical Radiology, 79*(8), 579–588. https://doi.org/10.1016/j.crad.2024.04.009

Pal, O. K., Danmusa, N. A., & Yusuff, H. D. (2024, July). bonenet: human bone fractures localising and diagnosing using hybrid neural network. In *2024 10th International Conference on Smart Computing and Communication (ICSCC)* (pp. 423–427). https://doi.org/10.1109/ICSCC62041.2024.10690459

Saraswat, A., Tooley, T., & Shrivastav, S. (2024). Osteoarthritis by deep learning approach. In A. Kalam, K. R. Niazi, A. Soni, S. A. Siddiqui, & A. Mundra (eds.), *Intelligent computing techniques for smart energy systems*. Springer.

Smith, T. O., Daniell, H., Geere, J. A., Toms, A. P., & Hing, C. B. (2012). The diagnostic accuracy of MRI for the detection of partial-and full-thickness rotator cuff tears in adults. *Magnetic resonance imaging*, *30*(3), 336-346.

Windarto, A. P., & Alkairi, P. (2024). Bone fracture classification using convolutional neural network architecture for high-accuracy image classification. *International Journal of Electrical & Computer Engineering, 14*(6), 2088–8708. https://doi.org/10.11591/ijece.v14i6.pp6466-6477

Xie, Z., Lu, Q., Guo, J., Lin, W., Ge, G., Tang, Y., ... & Wang, W. (2024). Semantic segmentation for tooth cracks using improved DeepLabv3+ model. *Heliyon, 10*(4). e25892. https://www.cell.com/heliyon/fulltext/S2405-8440(24)01923-6